Tryptophan-to-heme electron transfer in ferrous myoglobins

Roberto Monni, André Al Haddad, Frank van Mourik, Gerald Auböck, and Majed Chergui[1]

Laboratoire de Spectroscopie Ultrarapide, Institut de Sciences et Ingéniérie Chimiques, École Polytechnique Fédérale de Lausanne, CH-1015 Lausanne, Switzerland

Edited by Harry B. Gray, California Institute of Technology, Pasadena, CA, and approved March 31, 2015 (received for review December 5, 2014)

It was recently demonstrated that in ferric myoglobins (Mb) the fluorescence quenching of the photoexcited tryptophan 14 (*Trp^{14}) residue is in part due to an electron transfer to the heme porphyrin (porph), turning it to the ferrous state. However, the invariance of *Trp decay times in ferric and ferrous Mbs raises the question as to whether electron transfer may also be operative in the latter. Using UV pump/visible probe transient absorption, we show that this is indeed the case for deoxy-Mb. We observe that the reduction generates (with a yield of about 30%) a low-valence Fe–porphyrin π [Fe^{II}(porph$^{\bullet-}$)] -anion radical, which we observe for the first time to our knowledge under physiological conditions. We suggest that the pathway for the electron transfer proceeds via the leucine 69 (Leu^{69}) and valine 68 (Val^{68}) residues. The results on ferric Mbs and the present ones highlight the generality of Trp–porphyrin electron transfer in heme proteins.

electron transfer | heme proteins | tryptophan | picosecond | low valence heme

Electron transfer plays a fundamental role in many biological systems (1–3) ranging from photosynthetic proteins (4) to iron–sulfur (5), copper (6), and heme (7, 8) proteins. It was demonstrated that electron transfer can be used to produce from heme proteins in situ drugs with antimalarial activity (9) and it might have a role in protein folding (2). In general, electron transfer in proteins can occur over long distances (>10 Å) by hopping through different residues, thus reducing the time that would be needed for a single step tunneling from the donor to the acceptor (10–12). Aromatic amino acids and Tryptophan (Trp) in particular can act as a relay in such processes (13–19). Trp also acts as a phototriggered electron donor, e.g., in DNA repair by photolyase (16–18) and in cryptochromes (20, 21). When no obvious electron acceptors are present, excited Trp or (*Trp) still displays shorter lifetimes than its nanosecond decay times in solution (22, 23). This is due to its strong tendency to act as an electron donor, undergoing electron transfer toward the protein's backbone as in the case of apo-myoglobin mutants (24), small cyclic peptides (25), and human γ–D-crystallin (26). It is interesting to note that in wild-type horse heart (WT-HH) apo-myoglobin the fluorescence lifetime of the two *Trp residues was reported to be comparable to that in water (27), demonstrating the absence of deactivation mechanisms, either by energy or by electron transfer.

The protein visible absorption spectrum is dominated by their cofactors, e.g., heme or flavins, whereas the UV absorption in the region between 250 nm and 300 nm is mainly due to the three aromatic amino acids, Trp, tyrosine (Tyr), and phenylalanine (Phe) (28), with Trp having the highest molar extinction coefficient. The high sensitivity of Trp to the local environment and the possibility to correlate it with its fluorescence response (28) have led to its widespread use as a local natural probe of protein structure and dynamics in time-resolved fluorescence resonance energy transfer (FRET) studies, and it has emerged as the "spectroscopic ruler" in such studies (28–30). FRET is mediated by dipole–dipole coupling between a donor *Trp and an acceptor molecule, and its rate is inversely proportional to the sixth power of the distance between them and to the relative orientation of their dipoles.

Myoglobin (Mb) is a small heme protein composed of ∼150 residues (31) arranged in eight α-helices (from A to H) (*SI Appendix*, Fig. S7), whose biological function is to store molecular oxygen in muscles of vertebrates (32). This is accomplished by its prosthetic group: a Fe–Protoporphyrin IX complex bound to the protein structure via the proximal histidine (His^{93}) (*SI Appendix*, Fig. S7). Both ferric and ferrous hemes tend to bind small diatomic molecules (e.g., O_2, CO, NO, and CN) at the Fe site. Mb has two Trp residues that are situated in the α-helix A: Trp^7 toward the solvent and Trp^{14} within the protein and closer to the heme (*SI Appendix*, Fig. S7) (33). Previous time-resolved fluorescence studies on various Mb complexes have reported decay times (*SI Appendix*, Table S1) of ∼120 ps and ∼20 ps, for *Trp^7 and *Trp^{14}, respectively (34–38). These decay times appear invariant with respect to the ligand and the oxidation state of the iron ion in the heme. They were attributed to *Trp-to-porphyrin energy transfer via FRET over different donor–acceptor distances (37, 38) [the Trp^7-Heme and Trp^{14}-Heme center-to-center distances are 21.2 Å and 15.1 Å, respectively (33, 39) (*SI Appendix*, Fig. S7)]. We recently showed, using ultrafast 2D-UV and visible transient absorption (TA) spectroscopy, that in the ferric myoglobins (MbCN and MbH_2O) the relaxation pathway of *Trp^{14} involves not only a *Trp-to-heme FRET but also an electron transfer from the *Trp to the heme (40) in a ratio of approximately 60–40%. One can expect that due to its ferric character, the heme is a strong electron acceptor in these cases, and indeed our study showed the formation of an Fe^{II} heme.

However, the invariance of *Trp decay times in ferric and ferrous Mbs (*SI Appendix*, Table S1) suggests that similar electron transfer processes may also occur in ferrous Mbs. In this event, questions arise as to (*i*) whether a formally Fe^{I} heme is formed, which has to date been observed only in cryo-radiolysis experiments (41, 42), or (*ii*) whether the electron localizes on the porphyrin ring or even on the ligand that binds to the Fe ion. Theoretical investigations have suggested that an iron porphyrin anion radical can be formed (43–45).

Significance

We demonstrate the occurrence of tryptophan (Trp) to heme electron transfer (ET) in ferrous myoglobins by ultrafast UV spectroscopy. The ET gives rise to the theoretically predicted, low-valence Fe(II)(porph$^{\bullet-}$) anion radical, which we observe for the first time to our knowledge under physiological conditions. These results highlight the generality of Trp–porphyrin electron transfer events in heme proteins and question the systematic use of Trp fluorescence in FRET studies of protein dynamics.

Author contributions: M.C. designed research; R.M., A.A.H., F.v.M., and G.A. performed research; R.M., G.A., and M.C. analyzed data; and R.M., G.A., and M.C. wrote the paper.

The authors declare no conflict of interest.

This article is a PNAS Direct Submission.

Freely available online through the PNAS open access option.

[1]To whom correspondence should be addressed. Email: majed.chergui@epfl.ch.

This article contains supporting information online at www.pnas.org/lookup/suppl/doi:10.1073/pnas.1423186112/-/DCSupplemental.

To address these questions, here we present a UV-pump/visible-probe TA study of ferrous Mbs. In the latter case with apical diatomic ligands, e.g., MbNO and MbCO, heme photoexcitation leads to dissociation of the ligand, followed by its recombination to the heme, which can be both geminate (the ligand stays inside the protein scaffold) and nongeminate (the ligand migrates out of the protein scaffold) (46–48). For the NO ligand, recombination timescales are typically ∼10 ps, ∼30 ps, and ∼200 ps (46, 47), whereas for CO they span up to the millisecond range (46, 49–51). The presence of recombination timescales in the order of *Trp decay times leads to additional signal contributions, which complicate the analysis of the data. These problems are avoided using deoxy-Mb, which has a penta-coordinated heme bound only to the His^{93}. Upon heme photoexcitation, the system recovers to the ground state within a few picoseconds (46, 52). This allows investigating the *Trp–heme interaction without any overlapping contributions.

We show here that just as in the ferric Mbs (40), also in deoxy-Mb does $*Trp^{14}$ partly decay to the heme by electron transfer, competing with the FRET pathway. We find that the transferred electron is localized on the porphyrin ring, contrary to the ferric case where it resides on the metal center. This is due to the highly negative reduction potential of the Fe^{II}/Fe^{I} couple (53, 54), which is close to the porphyrin reduction potential (55). To our knowledge, this is the first report of a low-valent myoglobin, under physiological conditions.

The experimental setup, the sample preparation, and the data analysis are described in *SI Appendix*.

Results and Discussion

The static absorption spectra of deoxy-Mb and Trp (*SI Appendix*, Fig. S1) show that at wavelengths <310 nm, the contributions of the heme and Trp overlap, excluding selective excitation of the Trp residues. To disentangle the Trp and heme contributions we performed TA measurements exciting deoxy-Mb at 315 nm, where only the heme absorbs, and compared them to those exciting at 290 nm where both Trp and heme absorb. Assuming that the heme response is similar for both excitation wavelengths, this allows separation of the heme and the Trp contributions in the transient absorption signal. It must be noted that in the probe range used in our experiments (390–730 nm), Trp excited-state absorption (ESA) and stimulated emission (SE) as well as an eventual Trp–photoproduct absorption may contribute to the transient signal (22).

Photoexcitation at 315 nm. Fig. 1*A* shows TA spectra, at selected pump–probe time delays, obtained upon 315-nm excitation of deoxy-Mb (more TA spectra are shown in *SI Appendix*, Fig. S5). Two negative features appear at ∼430 nm and ∼550 nm that are due to ground state bleach (GSB) of the Soret and Q bands, respectively (*SI Appendix*, Fig. S1). Positive features due to ESA are observed at 450 nm and 600 nm, respectively (46, 52), which shift to the blue within the first 10–15 ps, while becoming weaker. The apparent shift of the GSB features results from the dynamics of the overlapping ESA contributions. Two mechanisms were proposed to explain the heme photocycle, namely the system undergoes vibrational relaxation (46, 52) or relaxes by cascading through spin states (56). However, our purpose here is not to discuss these mechanisms as they occur in the first few picoseconds or so and do not influence the *Trp kinetics we are investigating.

The timescales related to the relaxation of deoxy-Mb were retrieved by both a singular value decomposition (SVD) analysis and a global fit (GF). The fit function, used to recover the involved timescales, is a sum of exponential decays convoluted with the instrumental response function (IRF) (∼300 fs), assumed to be Gaussian. The timescales, obtained by a GF of the kinetic traces (*SI Appendix*, Fig. S3), are 280 ± 60 fs, 1.6 ± 0.2 ps, and 4.0 ± 0.4 ps, in agreement with the literature (49, 52, 56). The

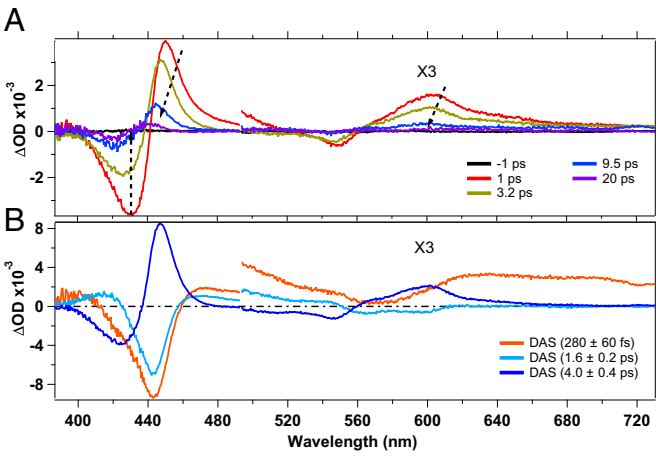

Fig. 1. (*A*) Transient absorption spectra at selected pump–probe delays of deoxy-Mb upon 315-nm photoexcitation. (*B*) Decay-associated spectra of the timescales obtained by an SVD analysis. The regions from 500 nm to 730 nm have been multiplied by 3.

large error for the 280-fs contribution results from its proximity to the duration of the IRF. In Fig. 1*B* we show the decay-associated spectra (DAS) obtained from the SVD analysis. The DASs are due to the amplitudes of the exponential decay functions used to best fit the data points, allowing us to define whether a certain feature is decaying or rising. A DAS is related to a particular timescale and it can be read by comparing it with the transient spectrum at the corresponding time delay. If the amplitude of the DAS has the same sign as the spectrum, the feature is decaying (e.g., a negative DAS in the GSB region), whereas if the DAS has opposite sign with respect to the spectrum, the spectral feature is rising (e.g., a negative DAS in the spectral region corresponding to an ESA feature).

As mentioned above, the interpretation of the mechanism related to the heme relaxation is still a subject of debate (46, 52, 56–58). Our aim here is not to discuss these mechanisms. Important is that the longest timescale in the heme photocycle is ∼4 ps, which is much shorter than the Trp decay times (∼20 ps and ∼120 ps).

Photoexcitation at 290 nm. Fig. 2*A* shows TA spectra at selected time delays, obtained upon 290-nm excitation (more TA spectra are shown in *SI Appendix*, Fig. S6). They display GSB features at ∼430 nm and 550 nm due to the Soret and Q bands, respectively. The latter is overlapped with a very broad unstructured positive contribution that we assign to ESA of the photoexcited Trp residues (22). Additionally the two ESA features of the heme (∼450 nm and ∼600 nm, corresponding to the Soret band and the Q band, respectively) are observed for small pump–probe delays. For time delays <15 ps, the TA spectra exhibit the same behavior as upon 315-nm excitation, namely the ESA features shift to the blue and decrease in intensity while the GSB decreases in intensity. However, at longer pump–probe delays the TA signals show a persistent GSB feature at ∼430 nm and two ESA features, at ∼460 nm and at ∼610 nm, respectively (Fig. 3). The TA spectra maintain the same shape from delay times of ∼40 ps up to 1 ns, except for a small reduction in intensity (over the entire probe range) in the first 100 ps due to the disappearance of the $*Trp^{14}$ and $*Trp^{7}$ ESA. Fig. 3 compares the TA spectra at 900 ps upon 315-nm (Fig. 3*A*) and 290-nm (Fig. 3*B*) excitation. The shape and the amplitude of these transients differ significantly, suggesting the formation of a long-lived (LL) photoproduct for 290-nm excitation. As this photoproduct spectrum displays clear features in the Soret- and Q-band region, it indicates a modification

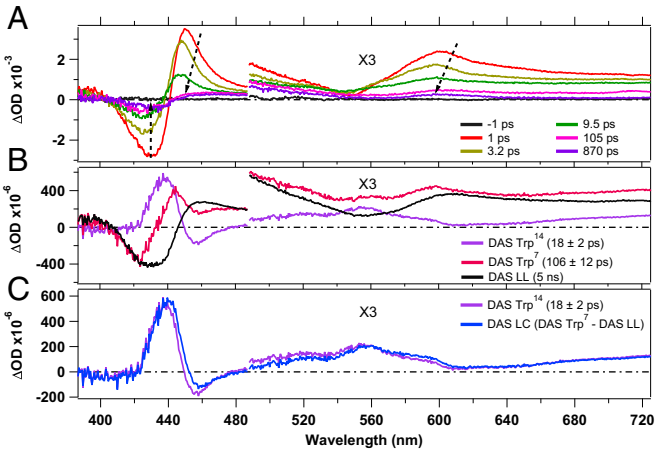

Fig. 2. (*A*) Transient absorption spectra, at selected pump–probe delays, of deoxy-Mb upon 290-nm photoexcitation. (*B*) DASs obtained by SVD analysis. (*C*) Comparison of the Trp^{14} DAS with the linear combination DAS LC = –LL DAS + DAS Trp^{7}. The regions above 500 nm are multiplied by 3.

of the heme group. Further, it cannot result from a *Trp–heme FRET process, because the heme photocycle is very short. The *Trp FRET rate would be the rate-limiting step and no LL photoproduct would be observed.

An SVD analysis and a GF (*SI Appendix*, Fig. S3) were performed to determine the kinetics of the spectral evolution. The fits, using six exponential components, yielded time constants of 230 ± 60 fs, 1.5 ± 0.2 ps, 4.4 ± 0.4 ps, 18 ± 2 ps, and 106 ± 12 ps and a long component (set to 5 ns) that accounts for the LL signal. All time constants (except for the 5 ns) were free parameters of the fit and the results are in excellent agreement with the decay times for the heme obtained upon 315-nm excitation (see above) and with the literature values for the *Trp decay times (35, 37).

Fig. 2*B* shows the DASs obtained for the $*Trp^{7}$ and $*Trp^{14}$ decay times (106 ps and 18 ps, respectively). Additionally the DAS corresponding to the LL photoproduct is shown (*SI Appendix*, Fig. S4 presents the full set of DASs). The DASs assigned to $*Trp^{7}$ and $*Trp^{14}$ decays differ significantly, indicating different relaxation pathways. The former contains a decay of the *Trp ESA as well as a response of the heme observed on the same timescale, because FRET is the rate-limiting step. The 18-ps DAS (Trp^{14}) is almost a mirror image of the LL DAS. More precisely, around 430 nm the positive feature in the Trp^{14} DAS mirrors the negative feature present in the LL DAS, although it is somewhat narrower. Furthermore, the two DASs mirror each other in the entire range from 460 nm to 730 nm, bearing in mind an overall small positive offset in the Trp^{14} DAS. This strongly suggests that $*Trp^{14}$ decay feeds the LL photoproduct population. The spectral response to excitation of the two Trp residues is likely similar, except for the rise of the photoproduct spectrum that occurs only upon excitation of the Trp^{14} residue. Thus, it should be possible to reproduce the Trp^{14} DAS with a linear combination (LC) of the Trp^{7} DAS, which represents the response from Trp excitation, and the inverted LL spectrum representing the rise of the photoproduct. This is shown in Fig. 2*C*, where we compare the linear combination –LL DAS + Trp^{7} DAS with the Trp^{14} DAS and find excellent agreement demonstrating that indeed, the LL state grows out of relaxation of the $*Trp^{14}$ residue.

As mentioned above, the LL photoproduct must be related to a change of the heme group and is not due to a *Trp-to-heme FRET. Because a phototriggered Trp^{14}-to-heme electron transfer was already reported for ferric Mbs (40) and because the *Trp decay times are almost invariant for all Mbs (*SI Appendix*, Table S1), this suggests that a photoinduced Trp^{14}-to-heme electron transfer also occurs in the ferrous deoxy-Mb. The resulting low-valent heme could be either an Fe^{I} heme or an Fe^{II}-porphyrin π-anion radical [$Fe^{II}(porph^{\bullet-})$] complex, if the additional electron resides on the porphyrin ring (59–63).

Several studies were performed, with a wide variety of techniques, on low-valent iron complexes, both as Fe^{I}–porphyrin and $Fe^{II}(porph^{\bullet-})$ (42, 53, 54, 60–64). However, a large part of these studies focuses on tetraphenyl-porphyrins (TPP) and octaethyl-porphyrins (OEP) in organic solvents (61, 64). It was concluded that formation of Fe^{I}–porph or $Fe^{II}(porph^{\bullet-})$ depends sensitively on the relative energy of the iron $d_{x^2-y^2}$ orbitals and the porphyrin e_g orbitals (*SI Appendix*, Scheme S1) (62). One way to experimentally affect the relative energies of these orbitals is substitution of the hydrogens in the porphyrin meso positions (e.g., in TPP and OEP) (62). If electron-withdrawing substituents are introduced in the ring, the energy of e_g orbitals will decrease, making the π-anion radicals more likely (62). On the other hand, if electron-donor groups are present in the ring, the energy of the e_g orbitals will become higher, leading to Fe^{I} complexes (62, 63, 65). In the case of the $Fe^{II}(porph^{\bullet-})$ species, absorption spectra display a broad band centered at ∼700 nm and ∼450 nm, and the Q and Soret bands disappear (62).

The LL photoproduct absorption spectrum (Fig. 3*C*) is obtained by subtracting the GSB contribution to the transient signal at 900 ps (Fig. 3*B*). It is comparable to the absorption spectrum of the reduced Fe^{II}-(NO_2-OEP), which generates a porphyrin π-anion radical (62), bearing in mind that this comparison is qualitative as the porphyrin, the solvent, and the environment differ. In Fig. 3*C*, the Soret band and the Q band are nearly vanished and new bands arise around 450 nm and 600 nm. This comparison leads us to conclude that the anion radical $Fe^{II}(porph^{\bullet-})$ is formed.

This is further supported by cryo-radiolysis experiments (41, 42). EPR/ENDOR studies of Mb at ∼70 K show that upon γ-ray irradiation, a mixture of Fe^{I}-Mb and $Fe^{II}(porph^{\bullet-})$-Mb is generated, in a 9:1 ratio (42). The authors suggested that different conformations in the frozen protein complexes might explain the simultaneous observation of both species. Annealing experiments hint at the possibility that the decay of Fe^{I} species could involve intramolecular electron transfer, leading to the formation of

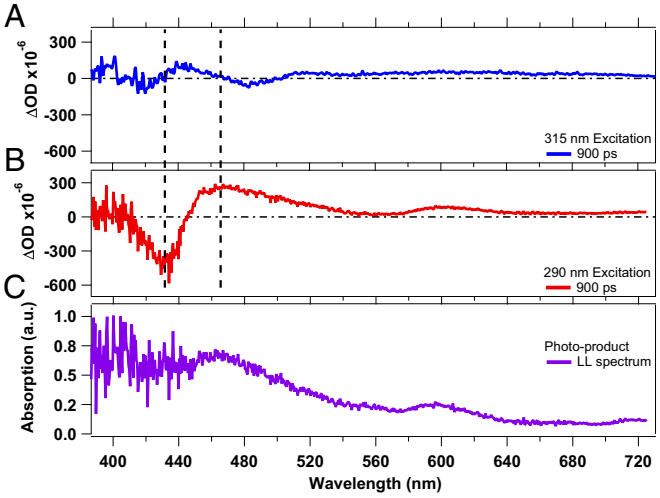

Fig. 3. Comparison of transient spectra of deoxy-Mb at 900 ps pump–probe delay time, obtained upon 315-nm (*A*) and 290-nm (*B*) excitation. *C* reports the spectrum of the LL photoproduct obtained by subtracting the bleach contribution from the LL transient shown in *B*.

$Fe^{II}(porph^{\bullet-})$ (42). The latter results suggest that the e_g and $d_{x^2-y^2}$ orbitals are close in energy, leading to the $Fe^{II}(porph^{\bullet-})$ when the system has the possibility to relax. Low-valent heme species, their nature, and relevance under physiological conditions were also investigated in theoretical studies (43–45), which also suggest formation of an $Fe^{II}(porph^{\bullet-})$.

The photoproducts of $^*Trp^{14}$-to-heme electron transfer can be $TrpH^{\bullet+}$ or $^*TrpH^{\bullet+}$ and $Fe^{II}(porph^{\bullet-})$ or $^*Fe^{II}(porph^{\bullet-})$. Because the transient spectra at delay times >40 ps do not display any changes (except for a small vertical offset due to $^*Trp^7$ and $^*Trp^{14}$ ESA), it is safe to assume that the $Fe^{II}(porph^{\bullet-})$ product is generated. In the opposite case [generation of $^*Fe^{II}(porph^{\bullet-})$] different spectral features should have been present in the transient spectra, together with their evolution. Further, if $TrpH^{\bullet+}$ is generated, an ESA feature at 560 nm [absorption band of $TrpH^{\bullet+}$ (66)] should arise with the $^*Trp^{14}$ decay time; if instead $^*TrpH^{\bullet+}$ is generated, some transient features should appear somewhere in the probing region (note that no information is available on $^*TrpH^{\bullet+}$ absorption bands, but an ESA feature should at least show up in the probed region). However, despite this fact, the transient spectra do not display any ESA feature around 560 nm, suggesting that the molar extinction coefficient of the generated $TrpH^{\bullet+}$ (or $^*TrpH^{\bullet+}$) is too small to detect the produced species. This is in line with the results on MbCN and met-Mb, in which the Trp radical cation was not detected either in its ground or in its excited state (40). Of course, if the signals of the products in their excited state fall outside the region of our probe and/or they decay to their ground state on a timescale that is too fast to be measurable with our setup, these considerations are no longer valid.

To estimate the quantum yield (QY) for electron transfer, the deoxy-Mb static spectrum (*SI Appendix*, Fig. S1) has been rescaled to the GSB amplitude of the LL transient spectrum at 900 ps, allowing a rough estimate of the proportion of Mbs with a $Fe^{II}(porph^{\bullet-})$ heme. The obtained value was divided by the total amount of excited Trp^{14} residues (details are given in *SI Appendix*). We find that ∼30% of photoexcited Trp^{14}s relax via electron transfer to the heme whereas the remaining ones relax via FRET. Because there are only these two parallel relaxation mechanisms, we can apply the relationship $QY = k_{et}/(\Sigma_i\, k_i)$ to obtain an estimate of the k_{et} leading to $k_{et} = 1/\tau_{et} = 1.7 \times 10^{-10}$ s^{-1} (τ_{et} = 60 ps). These values are similar to the ferric Mbs, where the QY was found to be ∼40% (40), implying $k_{et} = 1/\tau_{et} = 3.3 \times 10^{-10}$ s^{-1} (τ_{et} = 30 ps). More insights into the $^*Trp^{14}$-to-heme electron transfer reaction in ferrous Mbs could be obtained using Marcus theory (ref. 67 and *SI Appendix*, section *SII.4*). However, too many parameters are unknown in the present case, hindering a deeper analysis of the Marcus region in which this electron transfer occurs.

The reported absence of $^*Trp$ fluorescence quenching in apo-Mb (27) highlights the strong affinity of $^*Trp$ to undergo energy and electron transfer to the heme. Given the similarity in yields and timescales for ferric and ferrous Mbs, it seems that the $^*Trp$-to-heme electron transfer is not determined by the oxidation state of the iron ion, and therefore the interaction between $^*Trp$ and the porphyrin is the main cause for $^*Trp$ deactivation and thus for electron transfer to occur. We thus predict that in the ferric case, the prime acceptor of the electron is the porphyrin, even if at a subsequent stage it develops an Fe^{II} center.

Zhong and coworkers investigated Trp fluorescence quenching in proteins by interresidue and interhelical electron transfer and identified carbonyl- and sulfur-containing residues as quenching groups (24). Although a glutamic acid residue is present in the vicinity of Trp^{14} in Mb, it is oriented toward the solvent, so we do not consider it playing a role. Rather, we believe that a possible pathway for a single-step electron transfer from $^*Trp^{14}$ to the heme can involve Leu^{69}, which is in van der Waals contact with Trp^{14} and Val^{68} (*SI Appendix*, Fig. S7).

Having identified a Trp^{14}-to-heme electron transfer in ferric (40) and now in the ferrous deoxy-Mb and given the fact that the Trp fluorescence lifetimes are invariant in all Mbs (*SI Appendix*, Table S1), we anticipate the process to also be present in ligated ferrous Mbs. Hemoglobin (Hb) has six Trp residues: one in each α-subunit (α14) and two in each β-subunit (β15 and β37). Quite remarkably, their fluorescence lifetimes (68, 69) are comparable to the Mb values in *SI Appendix*, Table S1. As a matter of fact, in deoxy-, oxy-, and carboxy-Hb, the Trp residues are at typical distances of 13–18 Å from a heme porphyrin, which is comparable to the Trp^{14}–heme distance of 15.1 Å in Mb. We predict that a Trp-to-heme electron transfer also occurs in hemoglobins.

An extreme case of Trp fluorescence quenching in heme proteins was found for ferrous and ferric cytochrome *c* (Cyt *c*) with, respectively, decay times of 350 fs and 770 fs (57, 58). Trp is at van der Waals distances of the porphyrin (3–5 Å; *SI Appendix*, Fig. S8) in Cyt *c*, but the Trp quenching was clearly identified as being due to FRET, at least to 85%. In this case the FRET may well be mediated by an exchange (Dexter) mechanism, in which the donor loses an electron from its excited state that is donated back to its ground state by the acceptor. In the light of these and the present results, it seems that electron transfer can compete with FRET only when the latter is less efficient (due to distance and orientation of the donor/acceptor dipoles) and/or when residues between the Trp and the porphyrin are present that can mediate it. In any case, more studies are needed to fully understand the competition between FRET and electron transfer in hemoproteins.

Conclusions

Femtosecond UV-visible transient absorption experiments were performed on deoxy-Mb for excitation wavelengths near 300 nm. They reveal the formation of a long-lived photoproduct, which results from a $^*Trp^{14}$-to-heme electron transfer with a quantum yield of ∼30%. This species is an Fe^{II}–porphyrin π-anion radical that has a lifetime exceeding our measurement window of 1 ns. To our knowledge this is the first observation of such a low-valent heme complex under physiological conditions, although their existence and biological importance as intermediates in the production pathway of active species in cytochrome P450 (43) as well as for CO_2 reduction (44) were discussed earlier.

The similarity to our previous results on ferric Mbs (40) and the invariance of the $^*Trp$ lifetimes for all myoglobins suggests that the $^*Trp^{14}$-to-heme electron transfer is likely operative in the ligated ferrous Mbs.

We propose a single-step tunneling pathway for the electron transfer that involves the Leu^{69} and Val^{68} residues that lower the tunneling energy. Finally, as previously stressed (40, 70), care is advised when using $^*Trp$ fluorescence as a spectroscopic ruler, assuming that its fluorescence decay is due to FRET. This is surely an important tool in studies of protein dynamics but more often than previously thought, parallel electron transfer pathways may also contribute to its quenching.

Associated Content

Sample preparation, optical setup details, power dependence, data analysis details, and extra figures are available in *SI Appendix*.

ACKNOWLEDGMENTS. We thank Dr. Cristina Consani for useful discussions. This work was supported by the Swiss National Science Foundation via the National Centre for Competence in Research: Molecular Ultrafast Science and Technology.

1. Gray HB, Winkler JR (1996) Electron transfer in proteins. *Annu Rev Biochem* 65: 537–561.

2. Pascher T, Chesick JP, Winkler JR, Gray HB (1996) Protein folding triggered by electron transfer. *Science* 271(5255):1558–1560.

3. Cordes M, Giese B (2009) Electron transfer in peptides and proteins. *Chem Soc Rev* 38(4):892–901.
4. Rochaix JD (2011) Regulation of photosynthetic electron transport. *Biochim Biophys Acta* 1807(3):375–383.
5. Johnson DC, Dean DR, Smith AD, Johnson MK (2005) Structure, function, and formation of biological iron-sulfur clusters. *Annu Rev Biochem* 74:247–281.
6. Farver O, Pecht I (2011) Electron transfer in blue copper proteins. *Coord Chem Rev* 255(7-8):757–773.
7. Mines GA, Pascher T, Lee SC, Winkler JR, Gray HB (1996) Cytochrome c folding triggered by electron transfer. *Chem Biol* 3(6):491–497.
8. Schichman SA, Meyer TE, Gray HB (1996) Kinetics of electron transfer in Pseudomonas aeruginosa cytochrome cd(1)-nitrite reductase. *Inorg Chim Acta* 243(1–2):25–31.
9. Robert A, Benoit-Vical F, Meunier B (2005) The key role of heme to trigger the antimalarial activity of trioxanes. *Coord Chem Rev* 249(17–18):1927–1936.
10. Gray HB, Malmström BG (1989) Long-range electron transfer in multisite metalloproteins. *Biochemistry* 28(19):7499–7505.
11. Shih C, et al. (2008) Tryptophan-accelerated electron flow through proteins. *Science* 320(5884):1760–1762.
12. Gray HB, Winkler JR (2005) Long-range electron transfer. *Proc Natl Acad Sci USA* 102(10):3534–3539.
13. Farver O, et al. (1996) Structure-function correlation of intramolecular electron transfer in wild type and single-site mutated azurins. *Chem Phys* 204(2–3):271–277.
14. Blanco-Rodríguez AM, et al. (2011) Phototriggering electron flow through Re(I)-modified Pseudomonas aeruginosa azurins. *Chemistry* 17(19):5350–5361.
15. Lancaster KM, et al. (2011) Electron transfer reactivity of type zero Pseudomonas aeruginosa azurin. *J Am Chem Soc* 133(13):4865–4873.
16. Aubert C, Mathis P, Eker APM, Brettel K (1999) Intraprotein electron transfer between tyrosine and tryptophan in DNA photolyase from Anacystis nidulans. *Proc Natl Acad Sci USA* 96(10):5423–5427.
17. Aubert C, Vos MH, Mathis P, Eker APM, Brettel K (2000) Intraprotein radical transfer during photoactivation of DNA photolyase. *Nature* 405(6786):586–590.
18. Byrdin M, et al. (2004) Intraprotein electron transfer and proton dynamics during photoactivation of DNA photolyase from E. coli: Review and new insights from an "inverse" deuterium isotope effect. *Biochim Biophys Acta* 1655(1–3):64–70.
19. Wang M, Gao J, Müller P, Giese B (2009) Electron transfer in peptides with cysteine and methionine as relay amino acids. *Angew Chem Int Ed Engl* 48(23):4232–4234.
20. Giovani B, Byrdin M, Ahmad M, Brettel K (2003) Light-induced electron transfer in a cryptochrome blue-light photoreceptor. *Nat Struct Biol* 10(6):489–490.
21. Immeln D, Weigel A, Kottke T, Pérez Lustres JL (2012) Primary events in the blue light sensor plant cryptochrome: Intraprotein electron and proton transfer revealed by femtosecond spectroscopy. *J Am Chem Soc* 134(30):12536–12546.
22. Léonard J, Sharma D, Szafarowicz B, Torgasin K, Haacke S (2010) Formation dynamics and nature of tryptophan's primary photoproduct in aqueous solution. *Phys Chem Chem Phys* 12(48):15744–15750.
23. Fleming GR, et al. (1978) Nonexponential fluorescence decay of aqueous tryptophan and two related peptides by picosecond spectroscopy. *Proc Natl Acad Sci USA* 75(10): 4652–4656.
24. Qiu WH, et al. (2008) Ultrafast quenching of tryptophan fluorescence in proteins: Interresidue and intrahelical electron transfer. *Chem Phys* 350(1–3):154–164.
25. Pan CP, Barkley MD (2004) Conformational effects on tryptophan fluorescence in cyclic hexapeptides. *Biophys J* 86(6):3828–3835.
26. Chen J, Flaugh SL, Callis PR, King J (2006) Mechanism of the highly efficient quenching of tryptophan fluorescence in human gammaD-crystallin. *Biochemistry* 45(38):11552–11563.
27. Glandières JM, Twist C, Haouz A, Zentz C, Alpert B (2000) Resolved fluorescence of the two tryptophan residues in horse apomyoglobin. *Photochem Photobiol* 71(4):382–386.
28. Lakowicz JR (2006) *Principles of Fluorescence Spectroscopy* (Springer, New York), 3rd Ed, Chap 16.
29. Lakowicz JR (2006) *Principles of Fluorescence Spectroscopy* (Springer, New York), 3rd Ed, Chap 13.
30. Truong K, Ikura M (2001) The use of FRET imaging microscopy to detect protein-protein interactions and protein conformational changes in vivo. *Curr Opin Struct Biol* 11(5):573–578.
31. Hersleth HP, et al. (2007) Crystallographic and spectroscopic studies of peroxide-derived myoglobin compound II and occurrence of protonated FeIV O. *J Biol Chem* 282(32):23372–23386.
32. Ordway GA, Garry DJ (2004) Myoglobin: An essential hemoprotein in striated muscle. *J Exp Biol* 207(Pt 20):3441–3446.
33. Evans SV, Brayer GD (1988) Horse heart metmyoglobin. A 2.8-A resolution three-dimensional structure determination. *J Biol Chem* 263(9):4263–4268.
34. Janes SM, Holtom G, Ascenzi P, Brunori M, Hochstrasser RM (1987) Fluorescence and energy transfer of tryptophans in Aplysia myoglobin. *Biophys J* 51(4):653–660.
35. Willis KJ, Szabo AG, Zuker M, Ridgeway JM, Alpert B (1990) Fluorescence decay kinetics of the tryptophyl residues of myoglobin: Effect of heme ligation and evidence for discrete lifetime components. *Biochemistry* 29(22):5270–5275.
36. Willis KJ, Szabo AG, Krajcarski DT (1991) Fluorescence decay kinetics of the tryptophyl residues of myoglobin single-crystals. *J Am Chem Soc* 113(6):2000–2002.
37. Hochstrasser RM, Negus DK (1984) Picosecond fluorescence decay of tryptophans in myoglobin. *Proc Natl Acad Sci USA* 81(14):4399–4403.
38. Stevens JA, et al. (2010) Ultrafast dynamics of resonance energy transfer in myoglobin: Probing local conformation fluctuations. *J Phys Chem B* 114(3):1498–1505.
39. Phillips SEV, Schoenborn BP (1981) Neutron diffraction reveals oxygen-histidine hydrogen bond in oxymyoglobin. *Nature* 292(5818):81–82.
40. Consani C, Auböck G, van Mourik F, Chergui M (2013) Ultrafast tryptophan-to-heme electron transfer in myoglobins revealed by UV 2D spectroscopy. *Science* 339(6127): 1586–1589.
41. Davydov R, Osborne RL, Kim SH, Dawson JH, Hoffman BM (2008) EPR and ENDOR studies of cryoreduced compounds II of peroxidases and myoglobin. Proton-coupled electron transfer and protonation status of ferryl hemes. *Biochemistry* 47(18): 5147–5155.
42. Davydov R, Hoffman BM (2008) EPR and ENDOR studies of Fe(II) hemoproteins reduced and oxidized at 77 K. *J Biol Inorg Chem* 13(3):357–369.
43. Porro CS, Kumar D, de Visser SP (2009) Electronic properties of pentacoordinated heme complexes in cytochrome P450 enzymes: Search for an Fe(I) oxidation state. *Phys Chem Chem Phys* 11(43):10219–10226.
44. Kis Z, Silaghi-Dumitrescu R (2010) The electronic structure of biologically relevant Fe(0) systems. *Int J Quantum Chem* 110(10):1848–1856.
45. Silaghi-Dumitrescu R, Makarov SV (2010) A computational analysis of electromerism in hemoprotein Fe(I) models. *J Biol Inorg Chem* 15(6):977–986.
46. Ye X, Demidov A, Champion PM (2002) Measurements of the photodissociation quantum yields of MbNO and MbO(2) and the vibrational relaxation of the six-coordinate heme species. *J Am Chem Soc* 124(20):5914–5924.
47. Kruglik SG, et al. (2010) Picosecond primary structural transition of the heme is retarded after nitric oxide binding to heme proteins. *Proc Natl Acad Sci USA* 107(31): 13678–13683.
48. Petrich JW, et al. (1994) Ultrafast measurements of geminate recombination of NO with site-specific mutants of human myoglobin. *J Mol Biol* 238(3):437–444.
49. Tian WD, Sage JT, Srajer V, Champion PM (1992) Relaxation dynamics of myoglobin in solution. *Phys Rev Lett* 68(3):408–411.
50. Jackson TA, Lim M, Anfinrud PA (1994) Complex nonexponential relaxation in myoglobin after photodissociation of Mbco - measurement and analysis from 2-Ps to 56-Mu-S. *Chem Phys* 180(2–3):131–140.
51. Lim M, Jackson TA, Anfinrud PA (1997) Ultrafast rotation and trapping of carbon monoxide dissociated from myoglobin. *Nat Struct Biol* 4(3):209–214.
52. Kholodenko Y, Volk M, Gooding E, Hochstrasser RM (2000) Energy dissipation and relaxation processes in deoxy myoglobin after photoexcitation in the Soret region. *Chem Phys* 259(1):71–87.
53. Kadish KM, Larson G (1977) A study of the redox potentials and electron transfer rates of several naturally occurring and synthetic iron porphyrins in DMF. *Bioinorg Chem* 7(2):95–105.
54. De Silva C, Czarnecki K, Ryan MD (1999) Visible and resonance Raman spectra of low valent iron porphyrins. *Inorg Chim Acta* 287(1):21–26.
55. Kadish KM, van Caemelbecke E, Royal G (2000) Electron transfer. *The Porphyrin Handbook*, eds Kadisk KM, Smith KM, Guilard R (Academic, Orlando, FL), Vol 8.
56. Consani C, Auböck G, Bräm O, van Mourik F, Chergui M (2014) A cascade through spin states in the ultrafast haem relaxation of met-myoglobin. *J Chem Phys* 140(2):025103.
57. Consani C, Bram O, van Mourik F, Cannizzo A, Chergui M (2012) Energy transfer and relaxation mechanisms in Cytochrome c. *Chem Phys* 396:108–115.
58. Bräm O, Consani C, Cannizzo A, Chergui M (2011) Femtosecond UV studies of the electronic relaxation processes in Cytochrome c. *J Phys Chem B* 115(46):13723–13730.
59. Peychalh G, Wilson GS (1971) Electrochemical studies of some porphyrin Ix derivatives in aprotic media. *Anal Chem* 43(4):550–556.
60. Cohen IA, Ostfeld D, Lichtenstein B (1972) Characterization of a d iron system. Tetraphenylporphineiron (I) anion. *J Am Chem Soc* 94(13):4522–4525.
61. Lexa D, Momentea M, Mispelte J (1974) Characterization of reduction steps of Fe(Iii) porphyrins. *Biochim Biophys Acta* 338(1):151–163.
62. Yamaguchi K, Morishima I (1992) Low-valent iron porphyrins - Nmr evidence for Pi-anion-radical character in 2-electron-reduced iron(Iii) mesosubstituted or beta-pyrrole-substituted porphyrins. *Inorg Chem* 31(15):3216–3222.
63. Balducci G, Chottard G, Gueutin C, Lexa D, Saveant JM (1994) Electrochemistry of iron(I) porphyrins in the presence of carbon-monoxide - comparison with zinc porphyrins. *Inorg Chem* 33(9):1972–1978.
64. Donohoe RJ, Atamian M, Bocian DF (1987) Characterization of singly reduced iron(Ii) porphyrins. *J Am Chem Soc* 109(19):5593–5599.
65. Kadish KM, Bottomley LA (1977) Substituent effects on the formation constants of iron(III) and iron (II) tetraphenylporphyrin-pyridine complexes. *J Am Chem Soc* 99(7): 2380–2382.
66. Bellina B, et al. (2011) Spectroscopic signatures of peptides containing tryptophan radical cations. *Angew Chem Int Ed Engl* 50(48):11430–11432.
67. Marcus RA (1956) On the theory of oxidation-reduction reactions involving electron transfer. 1. *J Chem Phys* 24(5):966–978.
68. Bucci E, Malak H, Fronticelli C, Gryczynski I, Lakowicz JR (1988) Resolution of the lifetimes and correlation times of the intrinsic tryptophan fluorescence of human hemoglobin solutions using 2 GHz frequency-domain fluorometry. *J Biol Chem* 263(15):6972–6977.
69. Szabo AG, Willis KJ, Krajcarski DT, Alpert B (1989) Fluorescence decay parameters of tryptophan in a homogeneous preparation of human-hemoglobin. *Chem Phys Lett* 163(6):565–570.
70. Winkler JR (2013) Chemistry. FRETting over the spectroscopic ruler. *Science* 339(6127): 1530–1531.